Computers and Chemical Engineering 92 (2016) 180–188

Computers and Chemical Engineering

journal homepage: www.elsevier.com/locate/compchemeng

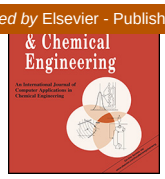

Circulating fluidized bed combustion reactor: Computational Particle Fluid Dynamic model validation and gas feed position optimization

R.K. Thapa[a,*], A. Frohner[b], G. Tondl[b], C. Pfeifer[b], B.M. Halvorsen[a]

[a] Institute for Process, Energy and Environmental Technology, Telemark University College, 3901 Porsgrunn, Norway
[b] University of Natural Resources and Life Sciences, Institute of Chemical and Energy Engineering, Muthgasse 107, A-1190 Vienna, Austria

ARTICLE INFO

Article history:
Received 7 March 2015
Received in revised form 21 April 2016
Accepted 15 May 2016
Available online 24 May 2016

Keywords:
CFB
Biomass gasification
Dual fluidized bed
CPFD

ABSTRACT

A 3D Computational Particle Fluid Dynamic (CPFD) model is validated against experimental measurements in a lab-scale cold flow model of a Circulating Fluidized Bed (CFB). The model prediction of pressure along the riser, downcomer and siphon as well as bed material circulation rates agree well with experimental measurements. Primary and secondary air feed positions were simulated by varying the positions along the height of the reactor to get optimum bed material circulation rate. The optimal ratio of the height of primary and secondary air feed positions to the total height of the riser are 0.125 and 0.375 respectively. The model is simulated for high-temperature conditions and for reacting flow including combustion reactions. At the high temperature and reaction conditions, the bed material circulation rate is decreased with the corresponding decrease in pressure drop throughout the CFB for the given air feed rate.

1. Introduction

Circulating fluidized bed reactors are widely used in various industrial applications including oxyfuel combustion, gasification and combustion of biomass or other carbonaceous feedstock. One of the applications of CFB in gasification processes is heating bed materials by combustion of fuels and then transporting them to the gasification reactor (Pfeifer et al., 2009). Fluid dynamic properties of the reactor, including gas-particle mixing and residence time, depend on the gas velocity and particle circulation rate for a given bed inventory (Ludlow et al., 2008). Gas velocity and bed material circulation rate are significant parameters determining the performance of the reactor. The solid circulation rate is also crucial for reaction kinetics. The solid circulation rate determines the fluid – solid contact time, heat transfer and overall performance of the CFB as a rector (Roy et al., 2001). The solid circulation rate and solid distribution over the circulating system are determined by the fluid dynamics (Lei and Horio, 1998) of the reactor. To obtain a proper distribution of the solids throughout the CFB, proper pressure balance is required (Kaiser et al., 2001). Improvement of performance of CFB mainly needs optimum fluid dynamic properties of the bed. Many researchers have studied the fluid dynamic behavior of CFB. Yerushalmi et al. have shown the transition between packed bed, bubbling bed, turbulent and fast fluidization regimes in the plot of bed voidage against superficial gas velocities (Yerushalmi et al., 1976). Flow regime maps of gas-solid flow are also developed plotting gas velocity against the solid flux (Leung, 1980). Takeuchi et al. performed experimental measurements to define the boundaries of fast fluidization (Takeuchi et al., 1986). Hirama et al. extended the flow diagram to transition from high velocity to low-velocity fluidization regimes (Hirama et al., 1992). Bi and Grace proposed unified flow regime diagram based on the experimental findings. They have shown the relationship between flow regimes for both gas-solid fluidization and co-current upward transport (Grace, 1986; Bi et al., 1993; Bi and Grace, 1995). In the all of the mentioned studies, the experiments are carried out at the ambient conditions. One of the significant factors affecting overall fluid dynamic properties of the bed is particle size distribution. The particle size distribution is not included in all the studies mentioned above. When particles of larger sizes and lower densities are mixed with the particles of smaller sizes and higher densities, the minimum fluidization velocity changes (Thapa et al., 2011). Change in minimum fluidization velocity effects on the transport velocity and fast fluidization velocity. High-temperature gasses have lower density and higher viscosity. Change in density and viscosity changes flow behavior in fluidized bed.

Therefore, the study of fluid dynamics in CFB should include the particle size distribution and the effect of high-temperature con-

* Corresponding author at: Kjølnes ring 56, P.O. BOX 203 N3901, Porsgrunn, Norway.
E-mail addresses: rajan.k.thapa@hit.no, rajankumarthapa@hotmail.com (R.K. Thapa).

http://dx.doi.org/10.1016/j.compchemeng.2016.05.008

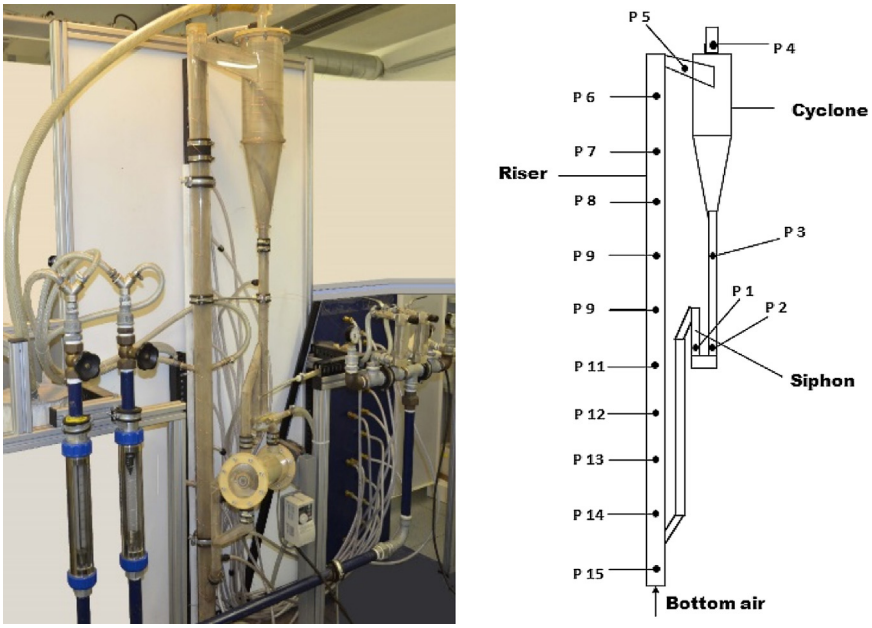

Fig. 1. (a) CFB cold model with air flow regulation and pressure measurement arrangements (b) pressure tapping points.

ditions. The gas-solid flow without chemical reaction differs from the reacting flow. The significance of those differences is not studied yet. The fluid dynamic properties of the CFB used in gasification of biomass is complicated due to the gas feed positions at different levels of the reactor. Air is fed to the reactor as bottom air at the bottom of the riser and primary and secondary air are fed along the height of the rector (Kaushal et al., 2008a,b). When the gas is fed at three positions of the bed, the feed position itself is expected to affect strongly on the fluid dynamics of the bed and the bed material circulation rate.

Design, scaling, operation and improvements of the circulating fluidized bed reactors require a good understanding of the fluid dynamic parameters affecting the performance (Gungor and Yildirim, 2013). Many of those parameters can be studied by the experimental investigations using laboratory models, pilot and demonstration plants. However, not all parameters are easy to study using experimental methods. For example, the study of the effect of the gas feed positions needs reconstruction of the reactor, which takes a lot of time and can be economically too costly. These facts indicate the usefulness of the computational models to overcome those types of challenges.

To overcome and/or substitute the experimental limitations, computer models have gained significant attention since the early 1990s. Computer models make it possible to study the fluid dynamics without disturbing the fluid flow field inside the reactor (Deen et al., 2007). The current work is therefore, focused on a validation of the CPFD (Computational Particle Fluid Dynamic) model against experimental measurements performed in a cold flow model of a CFB. The model is then used for further investigations of high temperature and reaction conditions as well as optimizing the feed positions of primary and secondary air.

2. Experimental set-up

The experimental rig is located at University of Natural Resources and Life Sciences (BOKU), Vienna, Austria. The set up consists of a cold model of a circulating fluidized bed as shown in Fig. 1. The model is made of a transparent Plexiglas, which makes it easier to visualize the fluidization and particle circulation during the experiments. The model is wrapped with conductive wires to avoid electrostatic forces at the wall. The fluidizing gas used in the experiment is ambient air supplied from a compressor. The fluidizing gas is fed as bottom air and primary air at two different stages of the reactor. The volume flow of primary and secondary air is measured through rotameters shown in Fig. 1a. The setup has 15 pressure tapping points which are connected to the pressure sensors. An industrial measurement and control system (B&R automation) is used to log the pressure data. The heights of pressure tapping points are shown in Table 1.

Table 1
Location of the pressure tapping points.

Labelling	Location	Height [mm]
P1	Siphon	665
P2	Siphon	665
P3	Downcomer	1010
P4	Exit Filter	1685
P5	Intersection Precipitator	1595
P6	Reactor	1535
P7	Reactor	1330
P8	Reactor	1170
P9	Reactor	1005
P10	Reactor	850
P11	Reactor	610
P12	Reactor	525
P13	Reactor	365
P14	Reactor	205
P15	Reactor	40

The siphon shown in Fig. 1b is also fluidized by air. The particles used in the experimental investigations are sand particles of density 2650 kg/m^3. The particle size distribution is presented in Fig. 2.

3. Computational model

In this work, a Computational Particle Fluid Dynamic (CPFD) model is used to simulate the gas-solid flow with heat transfer and chemical reactions. The commercial CPFD software Barracuda VR 15 is used for the simulations. The CPFD numerical methodology incorporates multi-phase-particle-in-cell (MP-PIC) method (Andrews and O'rourke, 1996; Snider, 2001). The gas phase is solved using the Eulerian approach and the particles are modeled

Table 2
Reactions and kinetics.

Reactions	Reaction rates	References
$2C(s)+O_2=2CO$	$r_1=4.34\cdot10^7\varepsilon_p Texp\left(-13519/T\right)[O_2]$	Snider et al. (2011)
$C(s)+H_2O=CO+H_2$	$r_2=1.272m_p Texp\left(-22645/T\right)[H_2O]$	Snider et al. (2011)
$H_2+0.5O_2=H_2O$	$r_3=1.63\cdot10^9T^{2/3}exp\left(-3420/T\right)[H_2]^{1.5}[O_2]$	Kaushal et al. (2007)
$CO+0.5O_2=CO_2$	$r_4=3.25\cdot10^7exp\left(-15098/T\right)[CO][O_2]^{0.5}[H_2O]^{0.5}$	Kaushal et al. (2007)
$CO+H_2O=CO_2+H_2$	$r_5=0.03exp\left(-20844/T\right)[CO][H_2O]$	Kaushal et al. (2007)

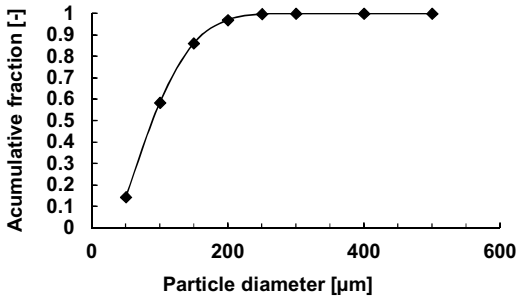

Fig. 2. Particle size distribution.

as Lagrangian computational particles. Gas and particle momentum equations are solved in three dimensions. The fluid is described by the Navier-Stokes equation with strong coupling to the discrete particles. The particle momentum follows the MP-PIC description which is a Lagrangian description of particle motions described by ordinary differential equations coupling with the fluid (Snider and Banerjee, 2010).

In the CPFD numerical method, actual particles are grouped into computational particles, each containing a number of particles with identical densities, volume and velocities located at a particular position. The computational particle is a numerical approximation similar to the numerical control volume where a spatial region has a single property for the fluid. With these computational particles, large commercial systems containing billions of particles can be simulated using millions of computational particles (Chen et al., 2013).

3.1. Governing equations

The volume averaged fluid mass and momentum equations are (Snider et al., 2011):

$$\frac{\partial\left(\varepsilon_g\rho_g\right)}{\partial t}+\nabla\left(\varepsilon_g\rho_g\boldsymbol{u}_g\right)=\delta\dot{m}_p \tag{1}$$

$$\frac{\partial\left(\varepsilon_g\rho_g\boldsymbol{u}_g\right)}{\partial t}+\nabla\left(\varepsilon_g\rho_g\boldsymbol{u}_g\boldsymbol{u}_g\right)=-\nabla p+\boldsymbol{F}+\varepsilon_g\rho_g\boldsymbol{g}+\nabla\varepsilon_g\tau_g \tag{2}$$

where ε_g, ρ_g and $\boldsymbol{u}_g$ are gas volume fraction, density and velocity respectively, p is gas pressure, $\mathbf{g}$ is the acceleration due to gravity, $\delta\dot{m}_p$ is the gas mass production rate per volume, $\boldsymbol{F}$ is the rate of momentum exchange per unit volume between the gas and solid phase and τ_g is stress tensor which can be expressed in index notation as:

$$\tau_{g,ij}=\mu\left(\frac{\partial u_i}{\partial x_j}+\frac{\partial u_j}{\partial x_i}\right)-\frac{2}{3}\mu\delta_{ij}\frac{\partial u_k}{\partial x_k} \tag{3}$$

where μ is shear viscosity. The shear viscosity is the sum of laminar shear viscosity and turbulence viscosity based on the Smagorinsky turbulence model. In the model, large eddies are directly calculated. The unresolved sub grid turbulence is modeled by using eddy viscosity. The turbulence viscosity is given as:

$$\mu_t=C\rho_g\Delta^2\sqrt{\left(\frac{\partial u_i}{\partial x_j}+\frac{\partial u_j}{\partial x_i}\right)^2} \tag{4}$$

where C is sub grid eddy coefficient and known as Smagorinsky coefficient.

The energy equation for the gas phase in terms of enthalpy equation for the gas mixture is given by:

$$\frac{\partial\left(\varepsilon_g\rho_g h_g\right)}{\partial t}+\nabla\cdot\left(\varepsilon_g\rho_g h_g\boldsymbol{u}_g\right)=\varepsilon_g\left(\frac{\partial p}{\partial t}+\boldsymbol{u}_g\cdot\nabla p\right)+\phi$$
$$-\nabla\cdot\left(\varepsilon_g\boldsymbol{q}\right)+\dot{Q}+S_h+q_{\dot{D}} \tag{5}$$

where h_g is the gas enthalpy, ϕ is viscous dissipation which is ignored in this work. $\dot{Q}$ is energy source per unit volume, which is zero in this work because there is no energy source. S_h is conservative energy exchange from solid phase to the gas phase and $\dot{q_D}$ is the enthalpy diffusion term. $\boldsymbol{q}$ is gas heat flux and is calculated as:

$$\boldsymbol{q}=\lambda_g\nabla T_g \tag{6}$$

where λ_g is thermal conductivity consisting a molecular conductivity (λ_m) and eddy conductivity (λ_t) from Reynolds stress mixing, related to Prandtl number as $Pr_t=\frac{C_p\mu_t}{\lambda_t}$. In this calculations $Pr_t=0.9$. T_g is the gas mixture temperature.

The gas mixture properties expressed in Eq. (5) are based on the mass fraction of gas species. The relation between mixture enthalpy and species enthalpy is given by:

$$h_g=\sum_{i=1}^{N}Y_{g,i}h_i \tag{7}$$

where $Y_{g,i}$ is the mass fraction of each gas species, h_i is species enthalpy. The species enthalpy depends on the gas temperature by:

$$h_i=\int_{T_0}^{T_g}C_{p,i}dT+\Delta h_{f,i} \tag{8}$$

where $\Delta h_{f,i}$ is the heat of formation at reference temperature T_0 and $C_{p,i}$ is specific heat at constant pressure for species i. The gas is compressible and pressure, enthalpy, temperature, density and mass fraction are related through equation of state. The pressure is given by the equation of state for the ideal gas as:

$$p=\rho_g RT_g\sum_{i=1}^{N}\frac{Y_{g,i}}{MW_i} \tag{9}$$

where R is universal gas constant, and MW_i is the molecular weight of gas species i.

The transport equation for the individual species in the gas phase is given by:

$$\frac{\partial\left(\varepsilon_g\rho_g Y_{g,i}\right)}{\partial t}+\nabla\left(\varepsilon_g\rho_g Y_{g,i}\boldsymbol{u}_g\right)=\nabla\cdot\left(\rho_g D\varepsilon_g\nabla Y_{g,i}\right)+\delta\dot{m}_{i,chem} \tag{10}$$

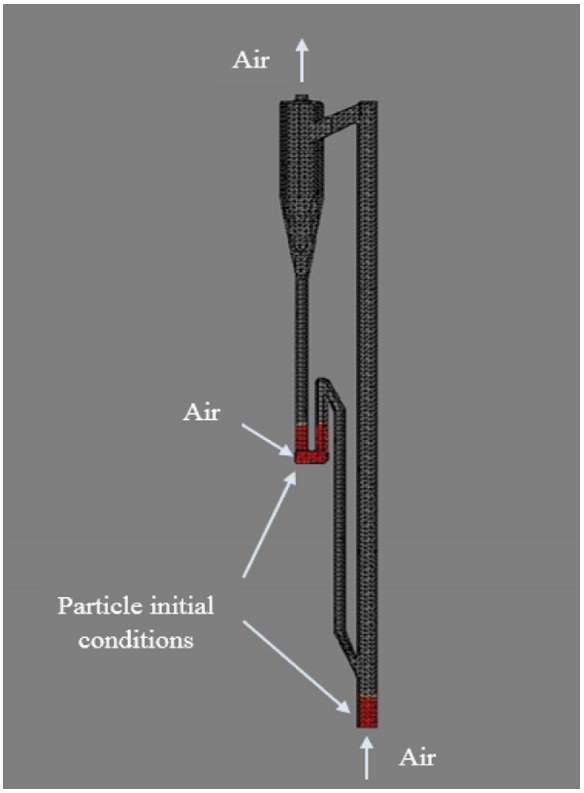

Fig. 3. Geometry and grid of simulated CFB – particle initial conditions.

Table 3
Simulation parameters.

Parameters	Units	Values
Reactor diameter	mm	50
Number of grids	–	53768
Initial time step	s	0.001
Mass of sand particles	kg	0.54
Mass of char particles	kg	0.014
Particle close pack volume fraction	–	0.6
Fluid feed temperature	K	300
Fluid and initial particle temperature:		
Ambient case	K	300
High temperature and reacting case	K	1073
Composition of air fed for combustion reaction:		
Nitrogen (N_2)	%	78.084
Oxygen (O_2)	%	20.9476
Argon (Ar)	%	0.9365
Carbon dioxide (CO_2)	%	0.0135

where $\delta\dot{m}_{i,chem}$ is the net production rate of species due to gas phase chemical reactions. D is the turbulent mass diffusion rate which is related to viscosity, μ_g by Schmidt number, Sc. The default value of Schmidt number is 0.9 in this work.

$$\frac{\mu_g}{\rho_g D} = Sc \tag{11}$$

The enthalpy diffusion term in Eq. (5) is given by:

$$\dot{\boldsymbol{q}}_D = \sum_{i=1}^{N} \nabla \cdot \left(h_i \varepsilon_g \rho_g D \nabla Y_{g,i} \right) \tag{12}$$

MP-PIC method calculates the particle phase dynamics for the particle distribution function, f_p. A transport equation is solved for

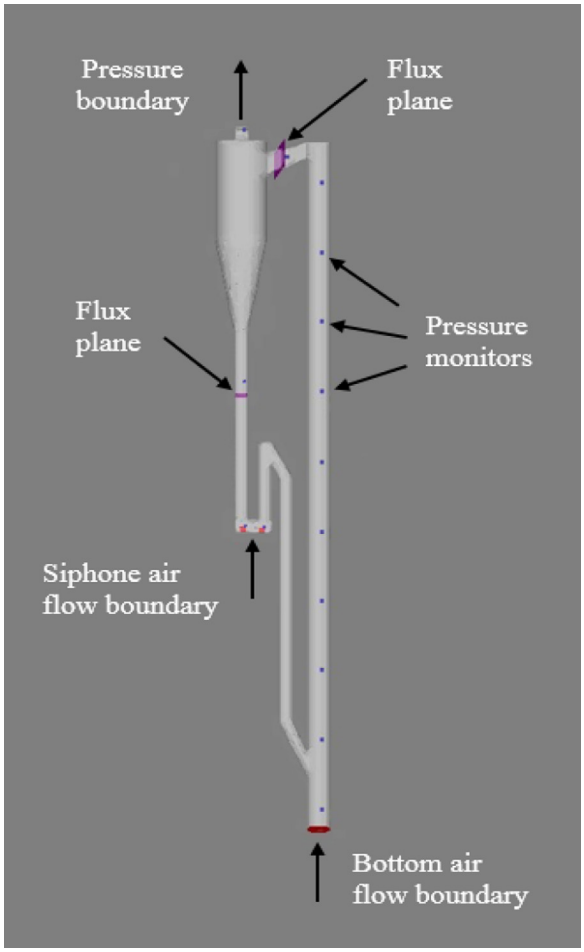

Fig. 4. Computational set up – pressure monitors and flux planes.

the Particle distribution function. The transport equation for f_p is given by (O'rourke and Snider, 2010)

$$\frac{df_p}{dt} + \frac{\partial \left(f_p \boldsymbol{u}_p\right)}{dx} + \frac{\partial \left(f_p \boldsymbol{A}_p\right)}{du_p} = \frac{f_D - f_p}{\tau_D} \tag{13}$$

where f_p is a function of the particle spatial location, $\boldsymbol{x}_p$, the particle velocity, $\boldsymbol{u}_p$, the particle mass, m_p, the particle temperature, T_p and the time, t. Therefore, $f_p\left(\boldsymbol{x}_p, \boldsymbol{u}_p, m_p, T_p, \mathrm{t}\right) d\boldsymbol{u}_p dm_p dT_p$ is the average number of particle per unit volume with velocities in interval $\left(\boldsymbol{u}_p, \boldsymbol{u}_p + d\boldsymbol{u}_p\right)$, masses in the interval $\left(m_p, m_p + dm_p\right)$ and temperatures in the interval $\left(T_p, T_p + dT_p\right)$. f_D is the particle distribution function for the local mass averaged particle velocity and τ_D is particle collision damping time(O'rourke and Snider, 2010). $\boldsymbol{A_p}$ is particle acceleration which is given by:

$$\boldsymbol{A_p} = \frac{d\boldsymbol{u}_p}{dt} = D_p\left(\boldsymbol{u}_g - \boldsymbol{u}_p\right) - \frac{1}{\rho_p}\nabla p_g + \boldsymbol{g} - \frac{1}{\varepsilon_p \rho_p}\nabla \tau_p + \boldsymbol{g} + \frac{\bar{\boldsymbol{u}}_p - \boldsymbol{u}_g}{\tau_D} \tag{14}$$

In the equation above, ε_p is the particle volume fraction, ρ_p is the particle density,p_g is the gas pressure, τ_p is the contact normal stress,$\bar{\boldsymbol{u}}_p$ is the local mass averaged particle velocity, and D_p is the drag function. The Wen-Yu drag model is used in this work (Wen and Yu, 1966).

$$D_p = C_D \frac{3}{8} \frac{\rho_g}{\rho_p} \frac{|\boldsymbol{u}_g - \boldsymbol{u}_p| \varepsilon_g^{-2.65}}{r_p} \tag{15}$$

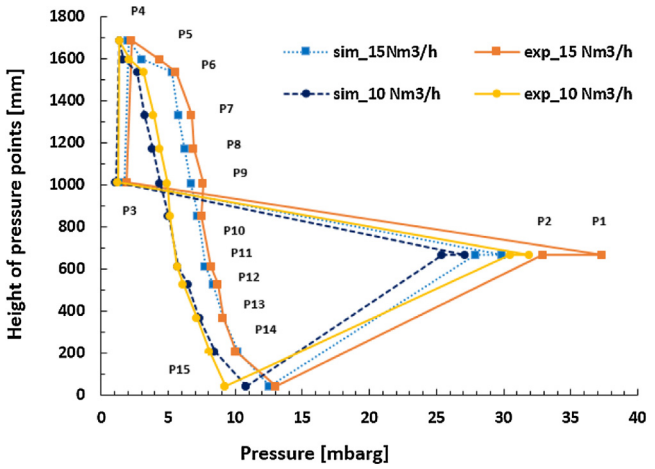

Fig. 5. Comparison of experimental and computational pressures.

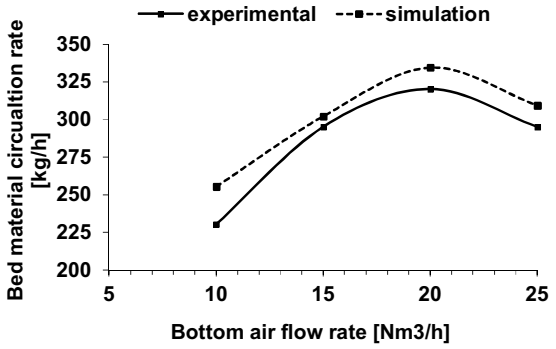

Fig. 6. Comparison of experimental and computational solid circulation rates as a function of bottom air feed rate.

where r_p is the particle radius and C_D is the drag coefficient. The drag coefficient is given by:

$$C_D = \begin{cases} \frac{24}{Re}\left(1 + 0.15Re^{0.687}\right) & Re < 1000 \\ 0.44 & Re \geq 1000 \end{cases} \quad (16)$$

where Re is the Reynold's number and is calculated as:

$$Re = \frac{\rho_g |\boldsymbol{u}_g - \boldsymbol{u}_p| r_p}{\mu_g} and r_p = \left(\frac{m_p}{\frac{4}{3}\pi\rho_p}\right)^{1/3} \quad (17)$$

The solid velocity is expressed as:

$$\frac{d\boldsymbol{x}_s}{dt} = u_p \quad (18)$$

The sum of the particle and gas volume fraction is unity and the particle volume fraction is related to the particle distribution function, f_p in the following way:

$$\varepsilon_p = -\iiint f_p \frac{m_p}{\rho_p} dm_p d\boldsymbol{u}_p dT_p \quad (19)$$

The interphase momentum transfer term, **F,** in Eq. (2) is defined by:

$$\boldsymbol{F} = -\iiint f_p \left\{ m_p \left[D_p \left(\boldsymbol{u}_g - \boldsymbol{u}_p\right) - \frac{\Delta p}{\rho_p} \right] + \boldsymbol{u}_p \frac{dm_p}{dt} \right\} dm_p d\boldsymbol{u}_p dT_p \quad (20)$$

In the MP-PIC method, the temperatures within the particle are assumed as uniform and there is no heat release within the parti-

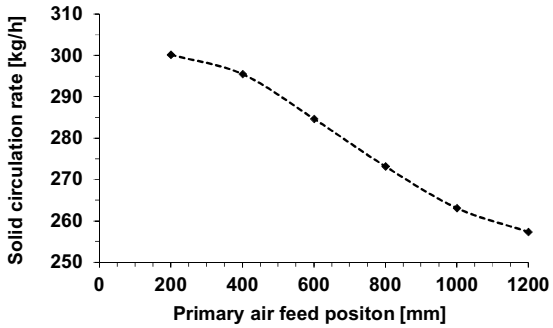

Fig. 7. Computational solid circulation rate vs. primary air feed position bottom air 15 Nm^3/h; primary air 5 Nm^3/h.

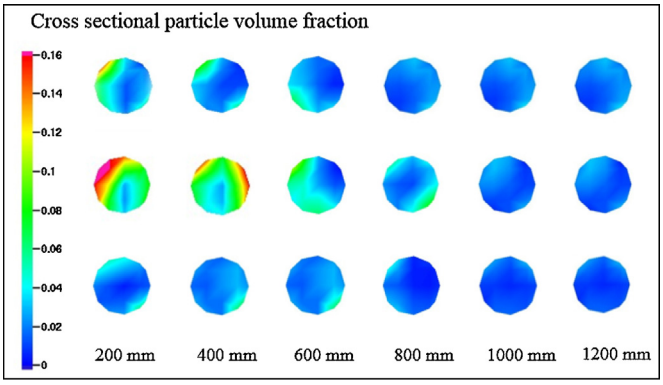

Fig. 8. Computational cross-sectional solid volume fractions.

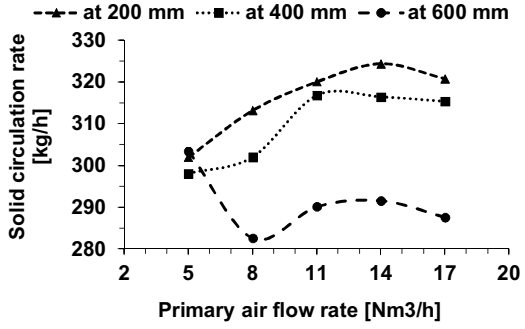

Fig. 9. Computational solid circulation rate vs. primary air flow rate at various feed positons.

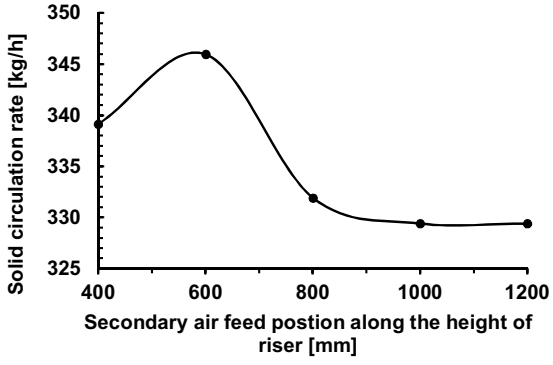

Fig. 10. Computational solid circulation rate vs. secondary air feed positon.

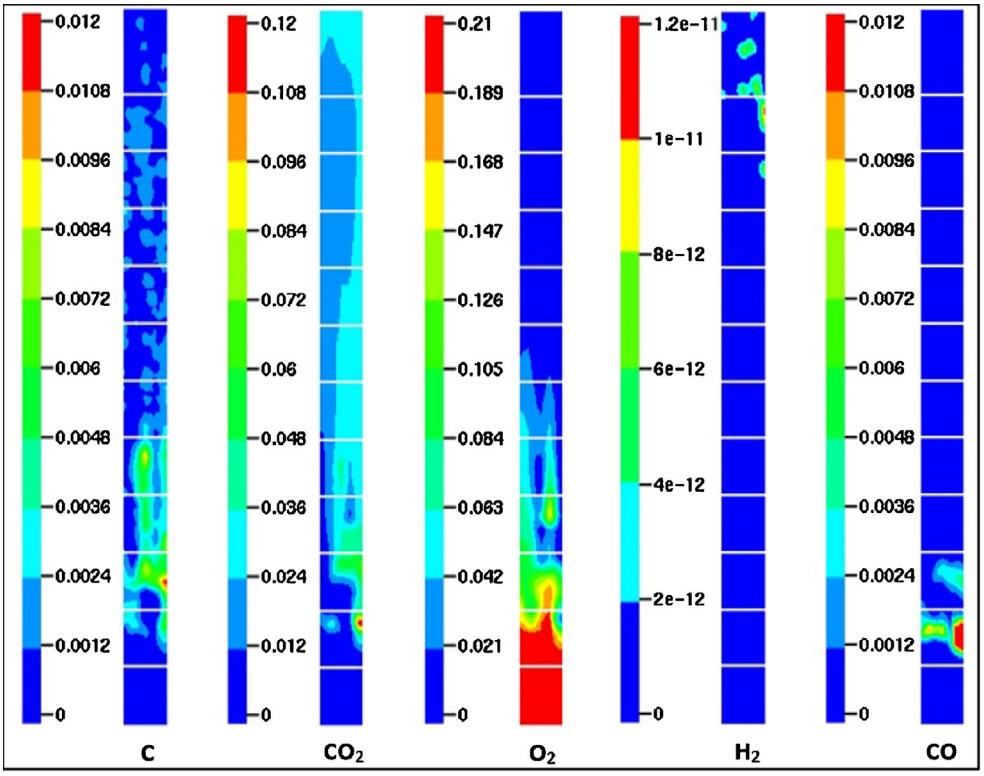

Fig. 11. Mole fraction of combustion products and char volume fraction.

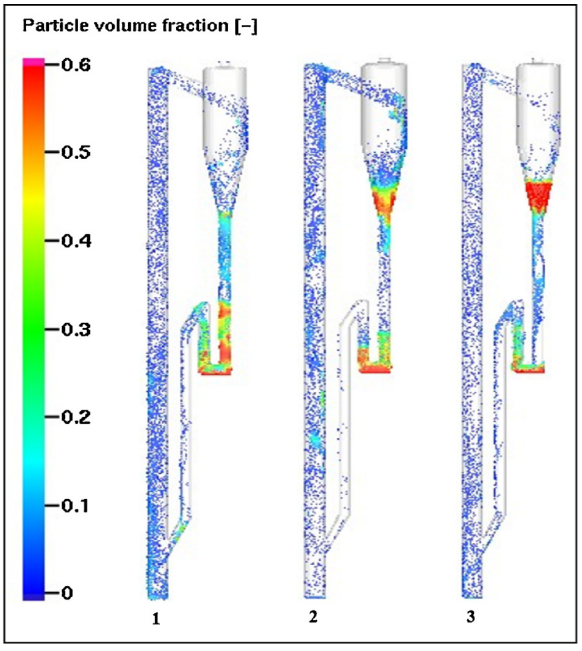

Fig. 12. Comparison of solid volume fraction throughout the CFB.

cle due to chemical reactions. It is assumed that the heat released due to chemical reactions on the surface of the particle does not contribute to the surface energy balance (Snider et al., 2011). The lumped heat equation for the particle phase is given by:

$$C_V \frac{dT_p}{dt} = \frac{1}{m_p} \frac{\lambda_g Nu_{g,p}}{2r_p} A_p \left(T_g - T_p\right) \tag{21}$$

where, C_V is the specific heat of particle, Nu_g is the Nusselt number for heat transfer from the gas to the particle. The conservative energy exchange term, S_h, in Eq. (5) is given by:

$$S_h = \iiint f_D \left\{ m_p \left[D_p \left(\boldsymbol{u}_p - \boldsymbol{u}_g\right)^2 - C_V \frac{dT_p}{dt} \right] - \frac{dm_p}{dt} \left[h_p + \frac{1}{2} \left(\boldsymbol{u}_p - \boldsymbol{u}_g\right)^2 \right] \right\} dm_p d\boldsymbol{u}_p dT_p \tag{22}$$

where h_p is the particle enthalpy. The terms $D_p\left(\boldsymbol{u}_p - \boldsymbol{u}_g\right)^2$ and $\left(\boldsymbol{u}_p - \boldsymbol{u}_g\right)^2$ are negligible in flow with low Mach number.

The chemistry in the CPFD model is specified as mass action kinetics. The chemical reactions are described by stoichiometric equations including the corresponding reaction kinetics. The reaction kinetics is expressed as:

$$k = A_0 m_p^{c1} T^{c2} \exp\left(-\frac{E}{RT} + E_0\right) \tag{23}$$

where A_0 is the pre-exponential factor, E is activation energy, E_0 is activation energy constant, R is universal gas constant, c is a constant. T is the temperature of a particle gas film. The film temperature is an average of the particle temperature and the bulk gas temperature. The particle concentration is given by mass per volume and $m_p = \rho_p \varepsilon_p$.

Only the basic governing equations for the gas and particles are described in this section. More details about the questions, their parameters and numerical procedures for solving the equations can be found in (Snider and Banerjee, 2010; Snider et al., 2011).

3.2. Model geometry and boundary conditions

The model geometry of the CFB reactor is designed to simulate the experimental situation. The geometry-grid used in the CPFD model is shown in Fig. 3. The air is introduced into the inlet boundaries. There are two fixed inlet (flow) boundaries – one at the bottom and another at the siphon. Air is introduced to both of the

boundaries at the same time. The air leaves at the outlet boundary located at the top of the reactor. Two more inlet boundaries are added as primary and secondary air along the height of the reactor for further computational investigations. The two additional air flow positions are only in computational studies and not the case of experimental investigations. The flow boundaries are different for different simulation cases, and they are therefore not shown in the figure. The heights of those boundaries are described in the relevant results and discussion sections. Initially, the particles are filled at the bottom and the siphon area of the reactor as shown in the figure.

The CPFD model contains the same number of pressure monitoring points as in the experimental study (P1-P15). The locations of the monitors are also the same as in experiments and are shown in Fig. 4. Two flux planes are set in the model to measure the solid circulation rate.

3.3. Gas-particle properties and chemical reactions

The particles used in the computational model are the same as the sand particles used in the experimental measurements. Ambient air is used as the fluidizing gas. To investigate hot flow and chemical reactions in the computational studies, char particles are mixed with the sand and the combustion reactions are introduced. The size distribution of char particles is also the same as sand particles given in Fig. 2. The ratio of char particles to sand particles is 1:40 by mass. The combustion reactions used in the model and their reaction kinetics are given in Table 2. Char particles are assumed as carbon which undergoes heterogeneous oxidation reaction with O_2 or with H_2O in the absence of O_2.

The aim of including the reactions in this work is to compare parameters such as particle circulation rate, the pressure drop along the height of the bed at ambient as well as high temperature reacting conditions.

Some of the parameters used as input to the simulations are given in Table 3.

4. Results and discussion

Experiments were performed in the lab-scale cold flow model with varying bottom air flow rate. Experimental pressure data measured via pressure tapping points are stored in an Excel data file for further processing. Pressure monitors are set in the computational model at the same locations as in experimental measurements. The experimental pressure measurements are compared with the computational prediction for two different air feed rates and are presented in Fig. 5.

The pressure is decreasing from bottom to top of the reactor (p15-p3). The computational pressure data deviate from experimental measurements by 0%–20% over the CFB reactor. The maximum deviations between experimental and computational data are in the siphon, and there are also some deviations at the top and the bottom of the reactor. Experimental measurements and simulations were also performed for higher feed rates. The deviations between experimental results and simulations show the same tendency at the higher air flow rates as well.

The particle circulation rates in the experimental study are determined by using the method of interruption of siphon fluidization. Initially, the particle height in the downcomer above the siphon is measured for a given air feed rate. Then the siphon fluidizing air flow is stopped abruptly for a given time. During that time, more particles are accumulated in the downcomer. The height is measured again. The difference between the two heights gives the height of accumulated particles. The circulation rate per time is determined based on the height of the particle accumulation and the cross-sectional area of the downcomer. Simulations were run for the same gas velocities. Solid circulation rates in the simulations are measured by using two flux planes as shown in Fig. 4. The simulation results of the solid circulation rates are compared with the experimental measurements. The results are presented in Fig. 6.

The deviation between experimental and computational results varies from 2% to 10%. Comparatively good agreements of the pressure and the solid circulation rates between the experimental and computational results give a basis for using the CPFD model for further investigation of the fluid dynamics of the circulating fluidized bed. Therefore, it is assumed that the further computational study of the CFB reactor without performing experimental measurements will give acceptable results.

Experimental investigation of the effect of the location of primary and secondary air feed can only be performed by reconstructing the rig which is both time consuming and economically costly. Therefore, further investigations are continued only with the CPFD model. In the CPFD model, the primary air flow is introduced together with the constant bottom air feed rate. Keeping both the bottom and the primary air feed rates constant, the primary air feed position is varied from the bottom of the riser by an interval of 200 mm. For all of the primary air feed positions, the total air feed rate in the simulations is constant, 20 Nm^3/h. The total air feed rate of 20 Nm^3/h is chosen, because the highest circulation rate is achieved at this feed rate as presented in Fig. 6. The riser fluidization determines the circulation rate in the system predominantly. However, siphon fluidization needs to be adjusted for optimum operation (Xu and Gao, 2003). For the given flow the siphon air feed of 1 Nm^3/h gives a stable circulation through the siphon. Solid circulation rate as a function of the primary air feed position is shown in Fig. 7. The solid circulation rate is decreasing with increasing height of primary air feed.

In Fig. 6, the bed material circulation rate at a bottom air flow rate of 20 Nm^3/h is about 335 kg/h. Fig. 7 shows that the maximum solid circulation rate is about 300 kg/h. When the gas is fed at two positons, the solid circulation rate is decreased even though the total gas feed rate is the same. The solid circulation rate decreases with increased height of the feed position of primary air from the bottom of the reactor.

Different cross-sectional particle volume fractions are presented in Fig. 8. The first row represents the cross-sectional volume fraction of particles when only the bottom air is fed to the riser. The cross sections are at the height of 200 mm to 1200 mm from the bottom with an interval of 200 mm and are presented in the figure as column 1–6 respectively. The first three cross sections have higher particle concentration, which indicates that the particle concentration is higher at the lower part of the riser than the upper part. The solid concentration is higher close to the wall than in the center.

The second and third row present the solid volume fractions when primary air is introduced into the reactor in addition to a constant feed of the bottom air. The second row shows the cross-sectional solid volume fraction just below the primary air feed position and the third-row present the solid volume fraction just above the primary air feed position. The first three columns show a large difference of cross-sectional volume fractions of particles below and above the primary air feed positions indicating that the introduction of primary air feed hinders the particles to flow upwards. The primary air is introduced at the side of the reactor. The introduction of the primary air feed, disturbs the particles upward flow, which is known as ‘cut off’ or ‘barrier’ effect (Koksal and Hamdullahpur, 2004). It is the reason of decreasing solid circulation rate with the introduction of the primary air flow. When air feed is located at a much higher position as indicated by column 4, 5, 6 in the figure, the solid concentration is not affected significantly. It may be due to the particle concentrations are very low at the higher location of the riser.

The model is used to investigate how the primary air feed rate effects on the bed material circulation rate. A series of simulations were run by gradually increasing the primary air feed rate. The set of simulations were repeated for the feed positions 200, 400 and 600 mm above the bottom air feed positions. Some of the results are presented in Fig. 9.

The solid circulation rate is increasing with the primary air flow rate up to the feed positon of 400 mm. At the higher feed positions, the solid circulation rates decrease. This result indicates that very high primary air feed positon is not suitable for the steady and maximized bed material circulation rate. The maximum solid circulation rate is achieved when the ratio of the height of the feed positon to the total height of the reactor is 0.125. The solid circulation rate is increasing with the primary air feed rate up to 14 Nm^3/h and then decreasing again.

Simulations were run to investigate the effect of the secondary air flow position on the bed material circulation rate. The bottom air feed is kept at 10 Nm^3/h and the primary air feed is maintained at the positon of 200 mm from the bottom with the feed rate of 14 Nm^3/h. These values are chosen because this combination gives the highest solid circulations rate. The secondary air flow rate is kept constant at 5 Nm^3/h and the feed positions are 400 mm, 600 mm, 800 mm, 1000 mm and 1200 mm. The bed material circulation rate as a function of secondary air flow position along the height of the reactor is shown in Fig. 10. The maximum solid circulation is achieved at the feed position at 600 mm from the bottom of the reactor. The ratio of the height of the feed position to the total height of the riser is 0.375.

A series of simulations were run to investigate the effect of increasing secondary air flow on the bed material circulation rate. The computational prediction shows that the bed material circulation rate is not affected significantly by the increasing secondary air feed rate.

The same feed rate of the bottom air as in the experimental measurements was used in the simulations with high temperature, initially without involving any combustion reactions. The high-temperature condition is simulated at the temperature of 800° C. High temperature makes change in density and viscosity of the fluidizing gas. The purpose of the simulation at high temperature without chemical reactions is to investigate the effect of density and viscosity of fluidizing gas on the solid circulation rate. Series of simulations were also run for the reacting flow including combustion of char particles. For the study of the combustion reaction, char particles are introduced to the reactor and mixed with bed material. The average reaction temperature is 800° C. The contours of the volume fraction of the char particles and mole fraction of the major gasses along the height of the reactor are shown in Fig. 11. The contour of the char volume fraction shows that there are some char particles present at the top of the riser. It indicates that there are some unreacted char particles circulating together with the sand particles. A mixture of two particles with different densities can affect flow behavior and consequently the particle circulation rate. Due to the chemical reactions, there is formation and consumption of gasses. The figure shows a significant amount of oxygen is present at the bottom part of the reactor which is not present at the top. It indicates that the oxygen gas is consumed at the bottom area of the reactor whereas the formation of CO_2 increases along the height of the reactor. The change in gas volume during flow along the reactor can also effect in particle circulation rate.

A series of simulations were run with constant air flow rate of 10 Nm^3/h to investigate the solid circulation rates at ambient condition, high-temperature condition and at high temperature with reactions. The solid volume fraction throughout the CFB at these conditions are presented in Fig. 12.

The contours presented in the figure are snapshots at time 100s. The contours 1, 2 and 3 are for the ambient, high temperature and reacting flow conditions respectively. The solid concentrations in the CFB are almost similar except for the high concentrations in the downcomer and cyclone separator in the case of flow at high temperature and flow with combustion reaction. The high concentration of particles in the downcomer for those two cases indicates decreasing solid circulation rates, which means that the siphon air flow rate and/or the cyclone capacity have to be increased. Contours of pressure for the corresponding simulations are shown in Fig. 13. The pressure drop throughout the CFB is less for the high temperature and reacting flow cases than for the case run at ambient conditions. From the results of solid volume fraction and pressure drop across the CFB, it is seen that the decreasing pressure drop over the CFB decreases the solid circulation rate if the siphon air flow rate remains constant.

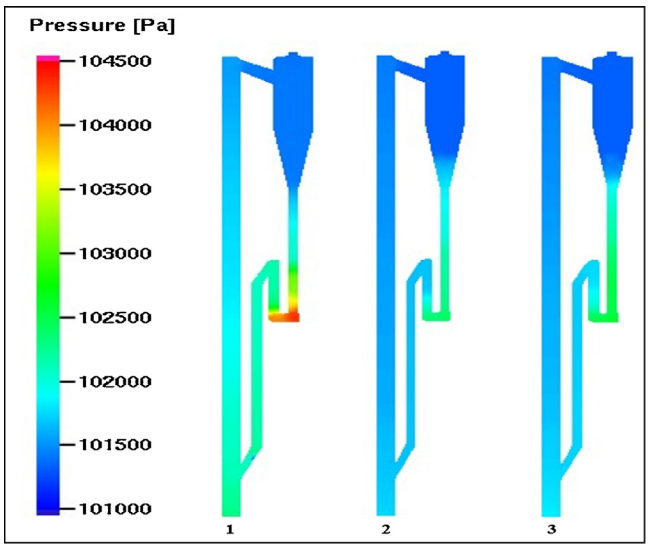

Fig. 13. Comparison of contours of pressure in CFB.

The solid circulation rates are 254 kg/h, 198 kg/h and 210 kg/h for the ambient, high temperature and reacting flow conditions respectively.

The difference in the flow properties at ambient conditions and high-temperature conditions are mainly due to the gas density and viscosity. At temperature 1073 K, the density of the air is decreased by four times and the viscosity is increased about two and a half time. Changes in density and viscosity change the flow behavior. The particles used in the current work, have small diameters and consequently they do not need high gas velocity for fluidization. The particle Reynolds number is 3.4, which is within the viscous dominated flow (Gidaspow, 1994). Viscosity plays a major role in this type of flow, and an increase in the viscosity decreases the minimum fluidization and transport velocity of the particles. The increase in viscosity may also be one of the reasons for the pressure decrease and consequently the decrease of solid circulation rate.

5. Conclusions

A 3D CPFD (Computational Particle Fluid Dynamic) model of a circulating fluidized bed (CFB) is validated against the experimental measurements in a lab-scale cold model. The pressure drops monitored in the CPFD model at a number of locations throughout the CFB are compared with the corresponding experimental measurements. The pressure deviation between experimental and computational results varies from 0% to 20% which is fairly well predicted. The model is simulated to measure the solid circulation rate at a series of varying air feed rates and the corresponding solid circulation rates are measured in the experiments. The deviation

between the computational prediction of solid circulation and corresponding experimental measurements at various air feed rates are from 2% to 10%.

The CPFD model is used to investigate the optimum primary and secondary air feed positions for maximum circulation rate of the bed material. The bed material circulation rate is maximum when the ratio of primary air feed position to the total height of the reactor is 0.125. The corresponding optimum ratio of secondary air feed position to the total height of the reactor is 0.375. At a given feed rate, the bed material circulation rate is decreasing when the air feed is split as the bottom, primary and secondary air. The circulation rate is highest when the total air is fed as bottom air.

Further investigation using the CPFD model shows that the particle circulation rate is decreased at high-temperature conditions and reacting flow conditions in comparison to the ambient flow conditions. The bed material circulation rates for ambient, high temperature and reacting flow conditions are 254 kg/h, 198 kg/h and 210 kg/h respectively at a total air flow rate of 10 Nm^3/h as bottom air.

The computational model is well predicting the flow behavior of the physical model and can be therefore used for optimization of the process.

References

Andrews, M.J., O'rourke, P.J., 1996. The multiphase particle-in-cell (MP-PIC) method for dense particle flow. Int. J. Multiphase Flow 22, 379–402.

Bi, H.T., Grace, J.R., 1995. Flow regime diagrams for gas-solid fluidization and upward transport. Int. J. Multiphase Flow 21, 1229–1236.

Bi, H.T., Grace, J.R., Zhu, J.X., 1993. Types of choking in vertical pneumatic systems. Int. J. Multiphase Flow 19, 1077–1092.

Chen, C., Werther, J., Heinrich, S., Qi, H.-Y., Hartge, E.-U., 2013. CPFD simulation of circulating fluidized bed risers. Powder Technol. 235, 238–247.

Deen, N.G., Van Sint Annaland, M., Van Der Hoef, M.A., Kuipers, J.A.M., 2007. Review of discrete particle modeling of fluidized beds. Chem. Eng. Sci. 62, 28–44.

Gidaspow, D., 1994. Multiphase Flow and Fluidization Continuum and Kinetic Theory Description. Academic Press, Boston.

Grace, J.R., 1986. Contacting models and behaviour classification of gas-solid and other two phase suspensions. Can. J. Chem. Eng. 64, 353–363.

Gungor, A., Yildirim, U., 2013. Two dimensional numerical computation of a circulating fluidized bed biomass gasifier. Comp. Chem. Eng. 48, 234–250.

Hirama, T., Takeuchi, H., Chiba, T., 1992. Regime classification of macroscopic gas–solid flow in a circulating fluidized bed riser. Powder Technol. 70, 215–222.

Kaiser, S., Weigl, K., Aichernig, C., Friedl, A., Hofbauer, H. Simulation of a highly efficient dual fluidized bed gasification process. Third European Congress on Chemical Engineering 2001 Nuernberg.

Kaushal, P., Pröll, T., Hofbauer, H., 2007. Model development and validation: co-combustion of residual char: gases and volatile fuels in the fast fluidized combustion chamber of a dual fluidized bed biomass gasifier. Fuel 86, 2687–2695.

Kaushal, P., Proll, T., Hofbauer, H., 2008a. Model for biomass char combustion in the riser of a dual fluidized bed gasification unit: part 1—model development and sensitivity analysis. Fuel Process. Technol. 89, 651–659.

Kaushal, P., Proll, T., Hofbauer, H., 2008b. Model for biomass char combustion in the riser of a dual fluidized bed gasification unit: part II—model validation and parameter variation. Fuel Process. Technol. 89, 660–666.

Koksal, M., Hamdullahpur, F., 2004. Gas mixing in circulating fluidized beds with secondary air injection. Chem. Eng. Res. Des. 82, 979–992.

Lei, H., Horio, M., 1998. A comprehensive pressure balance model of circulating fluidized beds. J. Chem. Eng. Jpn. 31, 83–94.

Leung, L.S., 1980. Vertical pneumatic conveying: a flow regime diagram and a review of choking versus non-choking systems. Powder Technol. 25, 185–190.

Ludlow, J.C., Monazam, E.R., Shadle, L.J., 2008. Improvement of continuous solid circulation rate measurement in a cold flow circulating fluidized bed. Powder Technol. 182, 379–387.

OO'rourke, P.J., Snider, D.M., 2010. An improved collision damping time for MP-PIC calculations of dense particle flows with applications to polydisperse sedimenting beds and colliding particle jets. Chem. Eng. Sci. 65, 6014–6028.

Pfeifer, C., Puchner, B., Hofbauer, H., 2009. Comparison of dual fluidized bed steam gasification of biomass with and without selective transport of CO2. Chem. Eng. Sci. 64, 5073–5083.

Roy, S., Kemoun, A., Al-Dahhan, M., Dudukovic, M.P., 2001. A method for estimating the solids circulation rate in a closed-loop circulating fluidized bed. Powder Technol. 121, 213–222.

Snider, D., Banerjee, S., 2010. Heterogeneous gas chemistry in the CPFD Eulerian–Lagrangian numerical scheme (ozone decomposition). Powder Technol. 199, 100–106.

Snider, D.M., Clark, S.M., O'rourke, P.J., 2011. Eulerian–Lagrangian method for three-dimensional thermal reacting flow with application to coal gasifiers. Chem. Eng. Sci. 66, 1285–1295.

Snider, D.M., 2001. An incompressible three-dimensional multiphase particle-in-cell model for dense particle flows. J. Comput. Phys. 170, 523–549.

Takeuchi, H., Hirama, T., Chiba, T., Biswas, J., Leung, L.S., 1986. A quantitative definition and flow regime diagram for fast fluidization. Powder Technol. 47, 195–199.

Thapa, R.K., Rautenbach, C., Halvorsen, B.M., 2011. Investigation of flow behavior in biomass gasfier using Electrical Capacitance Tomography (ECT) and pressure sensors. In: International Conference on Polygeneration Strategies (ICPS), Vienna, pp. 97–106.

Wen, C., Yu, Y., 1966. Mechanics of fluidization. Chem. Eng. Prog. Symp. Ser. 62, 100–111.

Xu, G., Gao, S., 2003. Necessary parameters for specifying the hydrodynamics of circulating fluidized bed risers—a review and reiteration. Powder Technol. 137, 63–76.

Yerushalmi, J., Turner, D.H., Squires, A.M., 1976. The fast fluidized bed. Ind. Eng. Chem. Process Des. Dev. 15, 47–53.